Magnetic properties of $LiCu_3O_3$: A quasi-two-dimensional antiferromagnet on a depleted square lattice

A. A. Bush [1], S. K. Gotovko [2,3], V. Yu. Ivanov [4], V. I. Kozlov [1,2], E. G. Nikolaev [2,*] and L. E. Svistov [2,†]

[1] *MIREA - Russian Technological University, Moscow 119454, Russia*

[2] *P.L. Kapitza Institute for Physical Problems, RAS, Moscow 119334, Russia*

[3] *National Research University Higher School of Economics, Moscow 101000, Russia*

[4] *Prokhorov General Physics Institute, RAS, Moscow 119991, Russia*

(Received 20 December 2023; accepted 28 February 2024; published 25 March 2024)

$LiCu_3O_3$ is a novel two-dimensional $S = 1/2$ antiferromagnet with randomly depleted square lattice. The crystal structure contains two types of square planes with different $Cu^{2+} \rightarrow Li^{+}$ substitution rates (20% and 40%). ^{7}Li NMR and magnetization measurements performed on single crystals of $LiCu_3O_3$ revealed the occurrence of magnetic order at $T_{c1} = 123$ K and the change of the magnetic state at $T_{c2} \approx 30$ K. The high-temperature transition can be attributed to establishment of magnetic order in planes with higher concentration of magnetic ions and the low-temperature transition to the magnetic ordering in planes with lower concentration of magnetic ions. Broad continuous NMR spectra below T_{c1} reflect a continuous distribution of values or directions of magnetic moments in $LiCu_3O_3$ typical for spiral, spin-modulated magnetic structures or structures with frozen disorder. Magnetization measurements revealed a spin-flop transition which indicates weak uniaxial anisotropy of the spin structure. The relatively small magnetic susceptibility at all orientations of applied magnetic field shows that the magnetic structure is rigid since the estimated value of saturation field derived from differential susceptibility measured at $\mu_0 H = 5$ T is $\mu_0 H_{sat} \approx 200$ T.

DOI: 10.1103/PhysRevB.109.115151

I. INTRODUCTION

Quasi-two-dimensional antiferromagnets on square lattice are of a great interest as experimental implementations of models in which the existence of various exotic magnetic states is predicted. Magnetic behavior of such objects is stipulated by the value of spins, hierarchy of exchange interactions of ions in sites of square lattice, and interaction with crystallographic surroundings. Nowadays, a big amount of such magnets with weakly bound crystallographic planes is known (see, for example, Refs. [1–5]). Particular interest is shown in strongly quantum case of spin $S = 1/2$ because quantum fluctuations play a crucial role in the choice of established magnetic states.

Naturally, various irregularities of square lattice significantly influence magnetic states. Particularly, special attention is drawn to substitution of magnetic ions with nonmagnetic impurities. Small dilution leads to change of boundaries of magnetic phase diagram, whereas the strong dilution can cause an occurrence of new exotic magnetic states. Such dilution decreases the spin stiffness, which can lead to an occurrence of microscopically nonuniform phases like frozen disorder or spin-glass state.

Models of diluted two-dimensional (2D) magnets on square lattice were considered in Refs. [6–9]. Experimentally, square lattice quantum antiferromagnets with different substitution degrees were studied in the systems $La_2Cu_{1-x}(Zn,Mg)_xO_4$ [5,10] and $Li_2V_{1-x}Ti_xOSiO_4$ [11]. Here we present a novel example of highly diluted square-lattice quantum antiferromagnetic (SLQAF) material $LiCu_3O_3$.

$LiCu_3O_3$ is a representative of a cuprate with mixed valency of copper ions: the number of magnetic Cu^{2+} ($S = 1/2$) ions is twice as much as the number of nonmagnetic Cu^{+} ions. The x-ray diffraction experiments on microcrystals of $LiCu_3O_3$ [12] show that the crystal structure of $LiCu_3O_3$ consists of four alternating square planes stacked along the C_4 axis: one square plane consists of Cu^{+} ions and other three square planes consist of $(Li^{+}, Cu^{2+})O^{2-}$ complexes. The sites of these three square planes are occupied by the nonmagnetic Li^{+} ions and magnetic Cu^{2+} ions statistically with proportion 1 to 2 to ensure electrical neutrality. Single-phase samples of $LiCu_3O_3$ crystals of millimeter size were grown recently [13]. The crystallographic structure of $LiCu_3O_3$ allows us to consider the magnetic material as an example of a highly diluted quasi-two-dimensional $S = 1/2$ magnet on a square lattice. Here we discuss the study of magnetic state of $LiCu_3O_3$ with magnetometry and NMR techniques. Two magnetic transitions were observed at $T_{c1} = 123$ K and $T_{c2} \approx 30$ K. In our report we suggest magnetic state of $LiCu_3O_3$ which can qualitatively describe the set of experimental data obtained.

II. CRYSTAL STRUCTURE OF $LiCu_3O_3$

At room temperature, the crystal structure of $LiCu_3O_3$ belongs to the space group P_4/mmm. The lattice

*nikolaev@kapitza.ras.ru

†svistov@kapitza.ras.ru

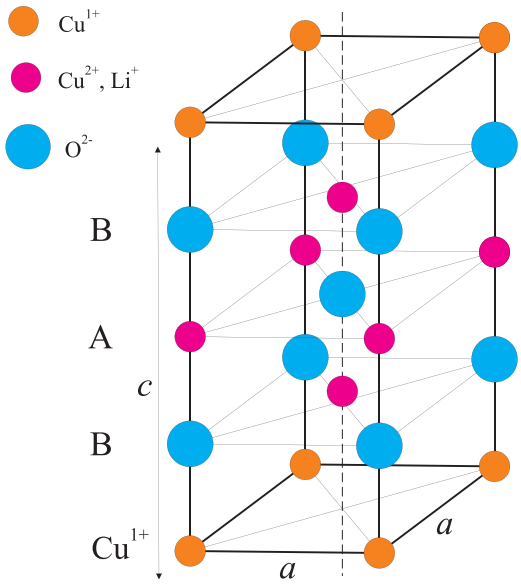

FIG. 1. Crystal structure of $LiCu_3O_3$. The smaller orange spheres mark the positions of the Cu^+ nonmagnetic ions, while the smaller magenta spheres in B, A, B square planes mark the positions of randomly distributed ions of nonmagnetic Li^+ and magnetic Cu^{2+}. The larger blue spheres are at the positions of the O^{2-} ions.

parameters of $LiCu_3O_3$ are $a = 2.810$ Å and $c = 8.889$ Å [12]. The crystal structure consists of alternating layers of Cu^+ ions and $(Li^+, Cu^{2+})O^{2-}$ complexes normal to the fourfold axis C_4. Within the layers, the crystal nodes form regular square lattices. Figure 1 shows the schema of crystallographic cell of $LiCu_3O_3$ drawn in accordance with the x-ray and neutron-diffraction experiments given in Refs. [12–14]. The planes of nonmagnetic Cu^+ ions are separated by three $(Li^+, Cu^{2+})O^{2-}$ square planes. The positions of Cu^+ and O^{2-} ions are shown in Fig. 1 with orange and blue circles, respectively. The positions of three intermediate planes colored with magenta are occupied by magnetic ions Cu^{2+} and nonmagnetic ions Li^+ statistically, forming the solid solution in these planes. The proportion of magnetic copper ions to lithium ions in central plane is 8:2, whereas for two outer planes the proportion is 6:4. In the following we denote the inner planes as A planes and outer planes as B planes.

The magnetic properties of $LiCu_3O_3$ crystals had not been studied before. We can do some comments concerning the expected magnetic structure of $LiCu_3O_3$ from considering its crystal structure. First, according to crystallography, the B-A-B triads of magnetic planes are separated by planes of nonmagnetic ions Cu^+. This fact can suggest their magnetic quasi-two-dimensionality. The quasi-2D magnetic behavior observed in related compound with mixed valency of copper $LiCu_2O_2$ [15] supports this assumption: in the case of $LiCu_2O_2$, nonmagnetic Cu^+ planes separate pairs of magnetic plains. The second very unusual and attractive feature of the crystal structure is random substitution of magnetic copper ions by nonmagnetic lithium ions: 20% for A planes and 40% for B planes. These are very high substitution levels, especially for 2D systems. The concentration of magnetic copper

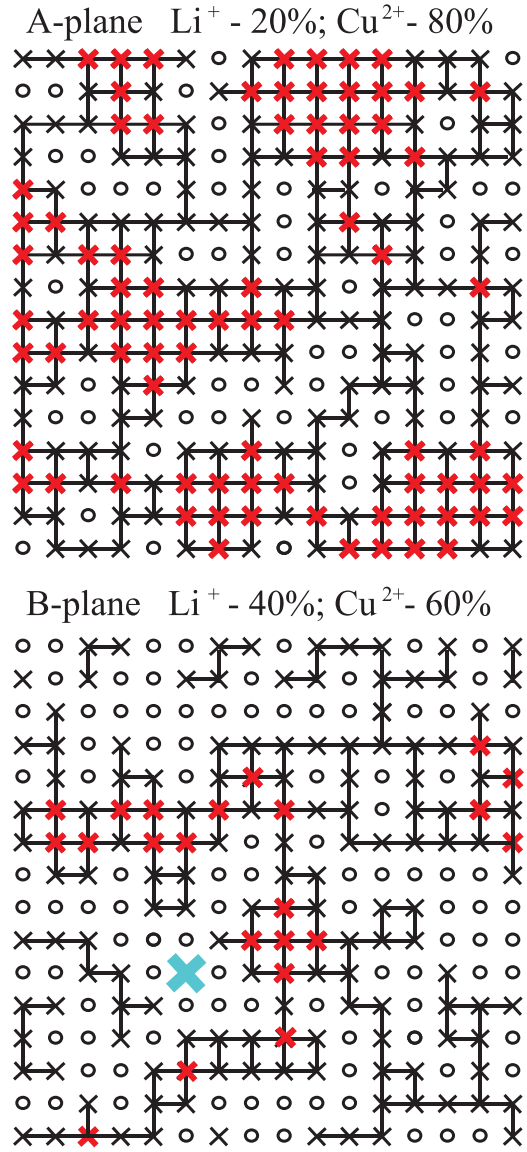

FIG. 2. Fragments of simulated square planes A and B with random occupation of crystal nodes of a regular square lattice by magnetic ions Cu^{2+} (crosses) and nonmagnetic Li^+ (circles). The bonds between nearest magnetic ions are shown with lines. Ions which have all four nearest magnetic neighbors are highlighted with bold red crosses. The ion which has no in-plane magnetic neighbors is highlighted with a bold blue cross.

ions in B planes is close to percolation threshold for a 2D square lattice [16]. For visualization, we generated two sets of square lattices with rates corresponding to A and B planes presented in Fig. 2. Copper ions are marked with crosses, and lithium ions are marked with circles. Lines show bonds between nearest magnetic ions. It can be seen that there is a very small number of magnetic ions with full set of in-plane magnetic neighbors: $0.8^5 = 0.32$ and $0.6^5 = 0.078$ for A and B planes, respectively. Such ions are colored with bold red crosses. It can be seen that the areas with regular bonds are coupled with net of "bridges" of ions with incomplete sets of exchange bonds. Not all magnetic copper ions have magnetic nearest neighbors: an example of such isolated ion is

marked in the Fig. 2(b) with bold blue cross. Concluding, we can expect, that magnetic state of $LiCu_3O_3$ is defined by the random distribution of in- and out-of-square-plane exchange interactions.

III. SAMPLE PREPARATION AND EXPERIMENTAL DETAILS

$LiCu_3O_3$ single crystals were grown from high-temperature solutions of Li_2CO_3 and CuO in an ambient atmosphere.

Crystal growth was conducted with flux method. Homogenized batch of $0.125 \cdot Li_2CO_3 \cdot 0.875 \cdot CuO$ was heated for three hours up to $T = 1270\,^{\circ}C$, which is higher than the melting point; then the melt was kept at this temperature for an hour; then it was cooled down to $T = 1090\,^{\circ}C$ in 30 minutes; after that, it was cooled down to $T = 915\,^{\circ}C$ in 50 hours; after keeping it at this temperature for 10 hours, the crystallized melt was rapidly cooled down to room temperature [13].

Typical dimensions of a crystal were $5\times5\times1$ mm^3 with the smallest side aligned with C_4 axis of the crystal. The developed planes of the plate were mirror-like smooth and had the shapes close to a rectangular with sides directed along [110] and [1−10] axes of the crystal. Unit cell parameters were in agreement with the previously reported [13]. The crystals of $LiCu_3O_3$ were stable in air and did not need any special precautions usually required for some other lithium and sodium cuprates.

The magnetization properties of $LiCu_3O_3$ were studied with use of commercial magnetometer MPMS-5XL (Quantum Design).

^{7}Li nuclei (nuclear spin $I = 3/2$, gyromagnetic ratio $\gamma = 16.5471$ MHz/T) were probed using the pulsed NMR technique. The spectra were obtained by summing fast Fourier transforms (FFT) of spin-echo signals as the frequency was swept through the resonance line. NMR spin echoes were obtained using $\tau_p - \tau_D - \tau_p$ pulse sequences, where the pulse lengths τ_p were 4–6 μs and the times between pulses τ_D were 30–60 μs. The measurements were carried out in the temperature range $4.2\ \mathrm{K} \leqslant T \leqslant 210\ \mathrm{K}$, temperature stability was better than 0.1 K.

IV. EXPERIMENTAL RESULTS

A. Magnetization measurements

Figures 3 and 4 show the temperature dependencies of magnetic susceptibility $\chi = M/\mu_0 H$ measured at fields $\mu_0 H = 1$ T and $\mu_0 H = 5$ T at **H** directed along and perpendicular to C_4 axis of the crystals, respectively. Magnetization in all figures is given in units of μ_B per one magnetic ion of Cu^{2+}, assuming that our samples are stoichiometric. Growth of susceptibility with temperature decrease is observed in the whole temperature range. The dependencies are well reproducible and no irreversibility or history effects have been observed. The temperature dependencies cannot be simply described by Curie-Weiss law: the reciprocal susceptibilities are not linear in studied temperature range (see insets to the top panels of Figs. 3 and 4). The high-temperature range can be roughly extrapolated by Curie-Weiss law with negative Curie-Weiss temperature $\Theta \approx -100$ K, which allows us to

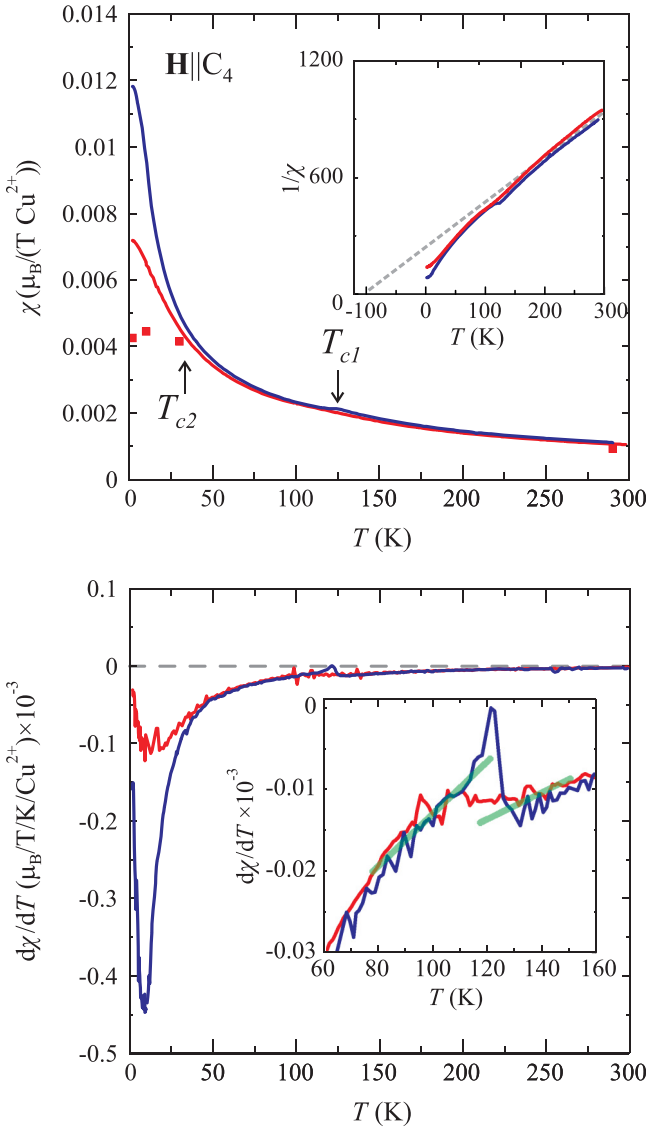

FIG. 3. (Top panel) Temperature dependence of magnetic susceptibility $\chi(T)$ of $LiCu_3O_3$ measured at $\mu_0 H = 1$ T (blue line) and $\mu_0 H = 5$ T (red line), $\mathbf{H} \parallel C_4$. Red squares show temperature dependence of the value of differential susceptibility obtained from $M(H)$ measurements at $\mu_0 H = 5$ T (see Fig. 5). Inverse susceptibilities $1/\chi(T)$ are shown in the inset to the Figure with respective colors. (Bottom panel) Temperature derivatives of $\chi(T)$ from the top panel. In the inset an expanded area in the vicinity of the singularity observed at $T \approx 120$ K is presented. Green solid lines mark the smoothed slopes of $\chi(T)$ at both sides of the critical point.

suppose the presence of strong dominant antiferromagnetic interaction in $LiCu_3O_3$. Against the background of susceptibility increase, a singularity at $T_{c1} = 120 \pm 10$ K is observed. This singularity is accompanied by sharp change in slope of susceptibility. $d\chi(T)/dT$ dependencies are shown in bottom panels of Figs. 3 and 4. The insets to the bottom panels of the figures show dependencies $d\chi(T)/dT$ expanded in the vicinity of the singularity at T_{c1}. Green solid lines show the smoothed dependencies above and below T_{c1}. In line with results of NMR experiments discussed below, we ascribe the singularity to partial antiferromagnetic ordering of

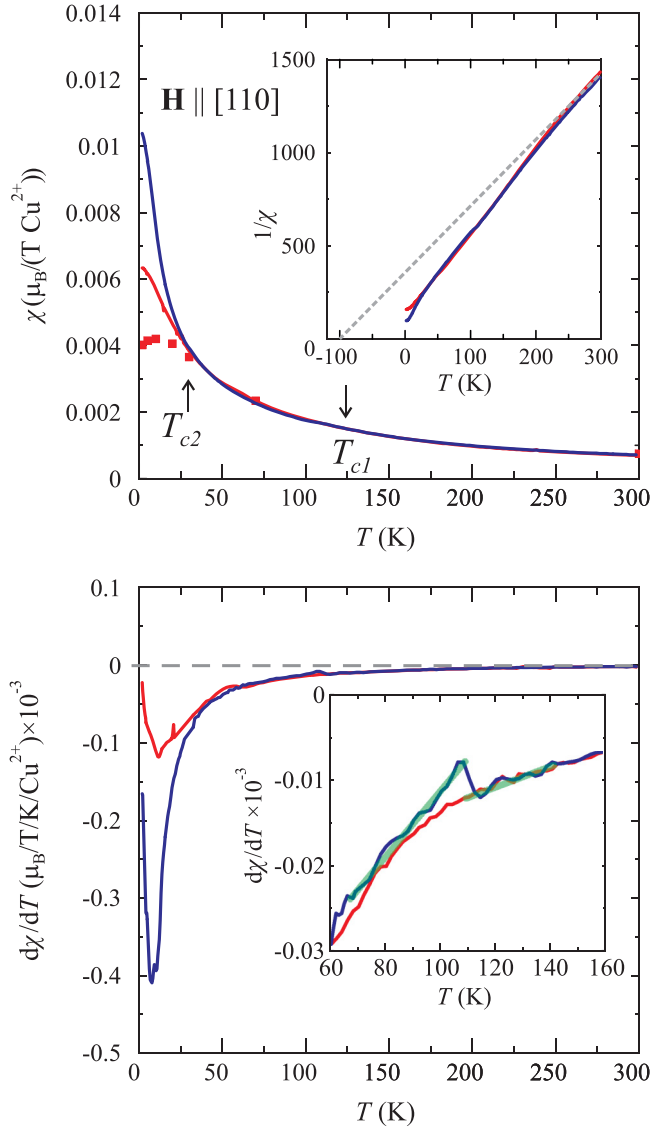

FIG. 4. (Top panel) Temperature dependence of magnetic susceptibility $\chi(T)$ of $LiCu_3O_3$ measured at $\mu_0 H = 1$ T (blue line) and $\mu_0 H = 5$ T (red line), $\mathbf{H} \perp C_4$. Red squares show temperature dependence of the value of differential susceptibility obtained from $M(H)$ measurements at $\mu_0 H = 5$ T (see Fig. 6). Inverse susceptibilities $1/\chi(T)$ are shown in the inset to the figure with respective colors. (Bottom panel) Temperature derivatives of $\chi(T)$ from top panel. In the inset an expanded area in the vicinity of the singularity observed at $T \approx 120$ K is presented. Green solid lines mark the smoothed slopes of $\chi(T)$ at both sides of the critical point.

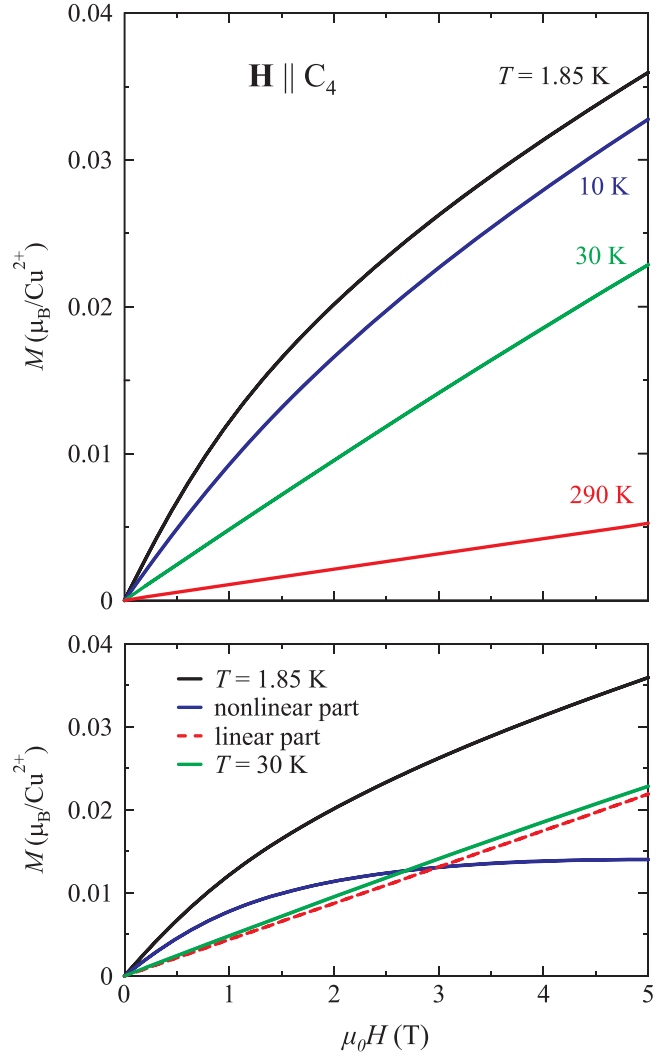

FIG. 5. (Top panel) Field dependence of magnetization M of $LiCu_3O_3$ measured at different temperatures, $\mathbf{H} \parallel C_4$. (bottom panel) $M(H)$ measured at $T = 1.85$ K (black line) and at $T = 30$ K (green line). Linear and nonlinear parts of $M(H, T = 1.85\ \text{K})$ obtained as described in the text are shown with dashed red and blue lines, respectively.

$LiCu_3O_3$. In this case, at lower temperature the susceptibility of ordered part stops its growth with temperature decrease, whereas the rest of the magnetic system continues to behave paramagnetically.

The temperature dependencies of susceptibilities measured at $\mu_0 H = 1$ T and $\mu_0 H = 5$ T are close at high temperatures, whereas at low temperatures they differ. This happens at temperatures below $T_{c2} \approx 30$ K. This is the marker of nonlinearity of magnetic moment dependence on magnetic field at low temperatures.

Field dependencies of magnetic moment of $LiCu_3O_3$ at different temperatures for fields parallel and perpendicular to the C_4 axis are shown in upper panels of Figs. 5 and 6. The dependencies are linear at temperatures higher than $T \approx 30$ K and nonlinear in the low-temperature range. The differential susceptibilities $d\chi/dH$ at high fields (≈5 T) for all curves measured below 30 K are nearly the same. The bottom panels of Figs. 5 and 6 show the results of separation of $M(H)$ at $T = 1.85$ K in a linear and a nonlinear parts: experimental black curve measured at 1.85 K can be presented as the sum of the linear part (dashed red line) and the nonlinear part (blue line). The linear part is close to $M(H)$ measured at 30 K. We ascribe the linear part of $M(H)$ below T_{c2} to magnetization of antiferromagnetically ordered fraction, and the nonlinear part to magnetization of the paramagnetic fraction. Note that the linear part of the susceptibility is weak: at $\mu_0 H = 5$ T, the value of magnetic moment M amounts to ≈2% of the

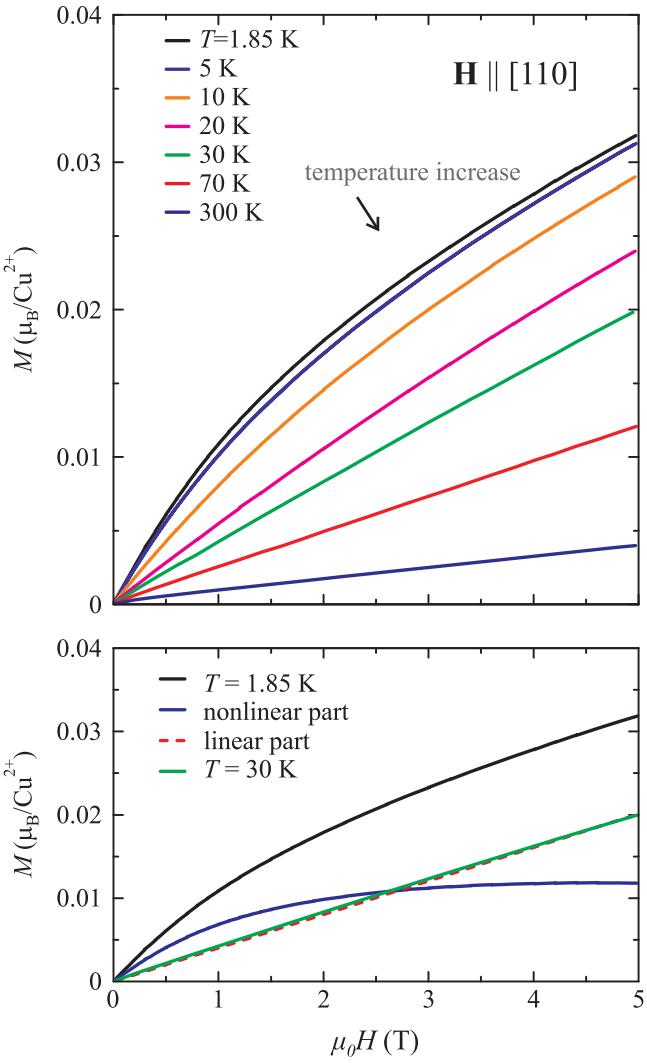

FIG. 6. (Top panel) Field dependence of magnetization M of $LiCu_3O_3$ measured at different temperatures, $\mathbf{H} \parallel [1\bar{1}0](\perp C_4)$. (bottom panel) $M(H)$ measured at $T = 1.85$ K (black line) and at $T = 30$ K (green line). Linear and nonlinear parts of $M(H, T = 1.85\ \text{K})$ obtained as described in the text are shown with dashed red and blue lines, respectively.

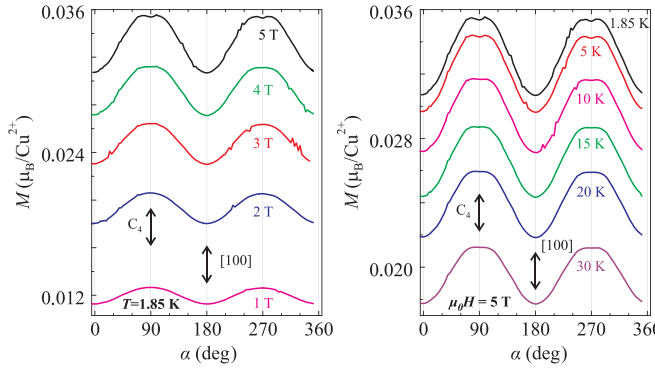

FIG. 7. (Left panel) Angle dependence of magnetization $M(\alpha)$ of $LiCu_3O_3$ measured at different values of $\mu_0 H$, $T = 1.85$ K. (Right panel) Angle dependence of magnetization $M(\alpha)$ of $LiCu_3O_3$ measured at different temperatures T, $\mu_0 H = 5$ T.

saturated value $gS\mu_B/Cu^{2+}$. The maximum contribution of the nonlinear part to full magnetization at the lowest temperature and $\mu_0 H = 5$ T is $\delta M \approx 0.012$–$0.014\ \mu_B/Cu^{2+}$ (see bottom panels in Figs. 5 and 6). This contribution can be reasonably explained by magnetization of the isolated magnetic ions discussed in Sec. II (bold blue cross in Fig. 2). The estimated portion of isolated Cu^{2+} ions is 1.6%, which is close to experimental value. Note that the similar nonlinear contribution to $M(H)$ was observed in weakly interacting antiferromagnetic nanoparticles [17].

The red squares in dependencies of $\chi(T)$ in Figs. 3 and 4 show the values of differential susceptibility dM/dH obtained from $M(H)$ measurements at $\mu_0 H = 5$ T, which are close to the linear part of susceptibility presumably defined by ordered magnetic fraction of $LiCu_3O_3$. The temperature at which the differential susceptibility measured at $\mu_0 H = 5$ T stops increasing is signed as $T_{c2} \approx 30$ K. Presumably, we associate this temperature with the ordering temperature of the residual portion of magnetic ions of $LiCu_3O_3$ which were not ordered at $T < T_{c1} = 123$ K.

The left panel of Fig. 7 shows angle dependencies of magnetic moment $M(\alpha)$ of $LiCu_3O_3$ measured at different values of magnetic fields at a constant temperature $T = 1.85$ K, where α is the angle between the [100] axis and the field direction. The field was rotated from the [100] axis to the C_4 axis of the crystal. The right panel of Fig. 7 shows the temperature evolution of $M(\alpha)$, measured at $\mu_0 H = 5$ T. In the whole studied field and temperature range, the susceptibility along C_4 exceeds the susceptibility in the plane (001) by $16 \pm 1\%$. This value can be explained by anisotropy of gyromagnetic ratio of Cu^{2+}. The close value of anisotropy of g factor was observed in related magnets $LiCu_2O_2$ and $LiCuVO_4$: $\Delta g/g \approx 10\%$ and 14%, respectively [18,19]. The left panel of Fig. 8 shows the angular dependencies of magnetization $M(\varphi)$ at $\mathbf{H}$ applied in the plane perpendicular to C_4. φ is the angle between the [110] axis and the field direction. $M(\varphi)$ were measured at different fields, $T = 1.85$ K. The angle-dependent part of susceptibility at all studied fields and temperatures does not exceed 3% of mean value. The angle-dependent part can be divided in two components: one harmonic component with period 180°, and another component with period 90° [see middle panel of Figs. 8(a)–8(c)]. Taking into account the crystal symmetry of $LiCu_3O_3$, the $\pi/2$ anisotropy seems to be natural. The harmonic modulation with a period of 180° we presumably associate with parasitic signal from the sample holder. The amplitude of this modulation was proportional to applied field. The right panel of Fig. 8 shows the dependencies given in the left panel of Fig. 8 with subtracted π harmonics. Next, we list the main features of the 90°-periodic parts of $M(\varphi)$. The maxima of magnetization is observed at $\mathbf{H}$ directed along square sides of crystal structure ($H \parallel$ [100], [010]). Attention is drawn to the sharp change in the sign of the slope to the left and to the right of the minimum. In the vicinity of the minima, the dependencies measured in the clockwise direction differ from the curve measured in the counterclockwise rotation. The arrows in the figure show the directions of field rotations. Slope singularity [see middle panel of Fig. 8(d)] and hysteresis mark the presence of the reorientation transitions at these

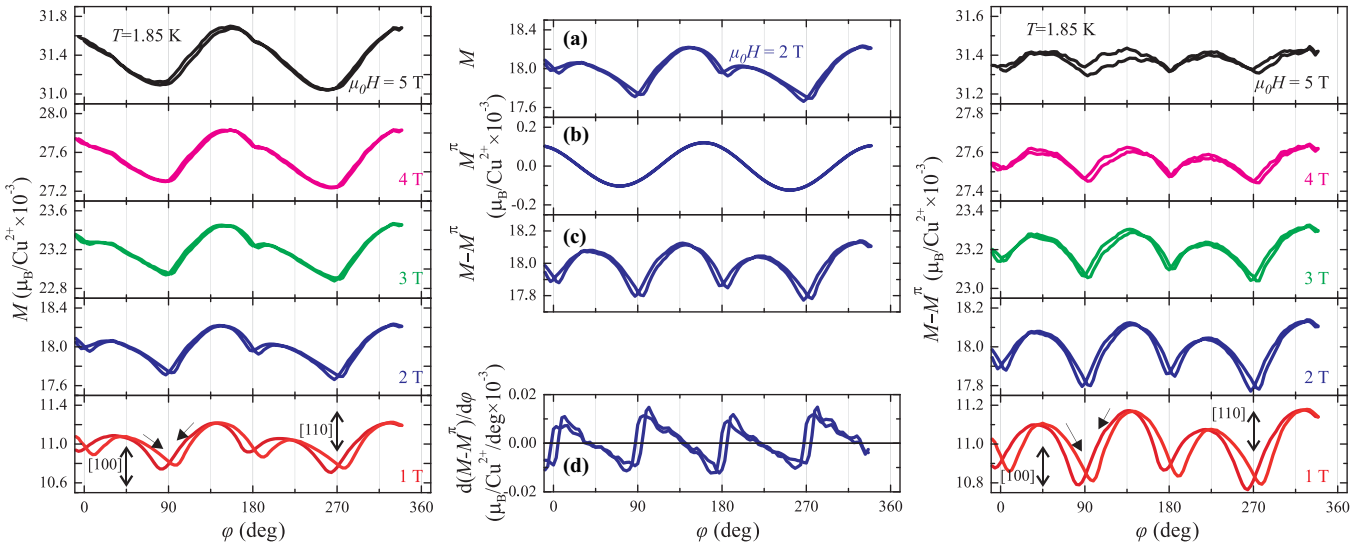

FIG. 8. (Left panel) Angle dependencies of magnetic moment M of $LiCu_3O_3$ measured at $\mu_0 H = 1 - 5$ T, $T = 1.85$ K. (Middle panel) (a) $M(\varphi)$ measured at $\mu_0 H = 2$ T. (b) π harmonic of $M(\varphi, \mu_0 H = 2\ \text{T})$ harmonic series. (c) Results of subtraction of π harmonic from $M(\varphi, \mu_0 H = 2\,T)$. (d) Angle derivative of $M(\varphi, \mu_0 H = 2\ \text{T}) - M^{\pi}(\varphi, \mu_0 H = 2\,T)$. (Right panel) Results of subtraction of second harmonics $M^{\pi}(\varphi)$ from magnetization measurements $M(\varphi)$. Arrows at the curves in the figure show the directions of field rotations.

angles. Such behavior is specific for exchange structures with axial symmetry such as collinear structure defined by vector of antiferromagnetism **l**, or planar spiral structure defined by vector **n** normal to the spin plane; for order parameters **l** or **n** there are strong easy-plane anisotropy within the (001) plane and weaker anisotropy within the easy plane. The examples of collinear and spiral antiferromagnets with such anisotropy hierarchy are well known (see, for instance, Refs. [20,21]).

B. Nuclear magnetic resonance

The ^{7}Li NMR spectra of $LiCu_3O_3$ were measured at the frequency scan around $\nu_0 = 30$ MHz at a permanent magnetic field equal to $\mu_0 H_0 = \nu_0/\gamma = 1.813$ T. Temperature evolutions of spectra for a field parallel and perpendicular to the crystal axis C_4 are shown in Fig. 9. At temperatures higher then ≈120 K, narrow NMR lines are observed. Lines obtained at H ∥ C_4 at $T = 207$ K demonstrate the quadrupole splitting of the central line of the ^{7}Li NMR spectra corresponding to the central transition $m_I = -1/2 \leftrightarrow +1/2$ and two satellites corresponding to the transitions $m_I = \pm 3/2 \leftrightarrow \pm 1/2$. The quadrupole splitting in $LiCu_3O_3$ is weak and will not be considered in the following discussion of the spectral broadening observed at low temperatures. The observed lines demonstrate the strong change in linewidth and lineshape at $T_{c1} \approx 123$ K. The mass center of observed spectra does not shift distinctly with temperature, which is in agreement with the small susceptibility of $LiCu_3O_3$ (see Figs. 5 and 6).

The temperature dependencies of linewidths $\delta\nu(T)$ measured at the 1/2 and 1/3 level of the maximal NMR signal at **H** parallel and perpendicular to C_4 are shown in Fig. 10. Temperature increase of $\delta\nu(T)$ measured at 30 K $< T < T_{c1}$ is proportional to $(1 - T^2/T_{c1}^2)^{\beta}$ (see solid lines in the figure). In our experiment, we obtain $\beta = 0.50 \pm 0.06$ for **H** ∥ C_4 and $\beta = 0.25 \pm 0.03$ for **H** ⊥ C_4. Experimentally observed disparity of exponents for different orientations of external magnetic field indicates that in-plane and out-of-plane components of magnetic moments order by different scenarios.

We associate the broadening of the NMR lines at $T < T_{c1}$ with the local magnetic fields from nearest ordered magnetic Cu^{2+} ions on the ^{7}Li nuclei. The broad spectrum signals a continuous distribution of local magnetic field values or directions on ^{7}Li positions with lifetime higher than time of NMR measurement. Note that broad continuous spectra are often found in incommensurate noncollinear spin structures [19,22].

Concluding, the abrupt broadenings of ^{7}Li NMR line take place at $T_1 \approx 123$ K and $T_2 \approx 30$ K, which is in agreement with singularities on $M(T)$ observed at T_{c1}, T_{c2}. The shape of the ^{7}Li spectra indicates continuous distribution of values or directions of Cu^{2+} magnetic moments in the magnetically ordered state.

V. DISCUSSION

We start the discussion from the model of infinite square lattice with sites occupied by magnetic ions of Cu^{2+} ($S = 1/2$) with the dominant in-plane exchange interactions along the sides and diagonals of squares J_1 and J_2, respectively, hoping that this rough model can explain several observations.

Taking into account the results of magnetization measurements, we can consider that the dominant exchange interaction is antiferromagnetic and, as a result, in the large-spin limit, we can expect the long-range order to be antiferromagnetic. If the exchange interaction along square sides, J_1, is dominant, the wave vector of the magnetic structure is $\mathbf{q} = [\pi, \pi]$. In case the dominant diagonal interaction is J_2, the structures with $\mathbf{q} = [\pi, 0]$ are expected. In the quantum case of $S = 1/2$, corresponding short-range correlations are expected. The model phase diagram for the large-spin limit and $S = 1/2$ for 2D model was considered in Refs. [23,24].

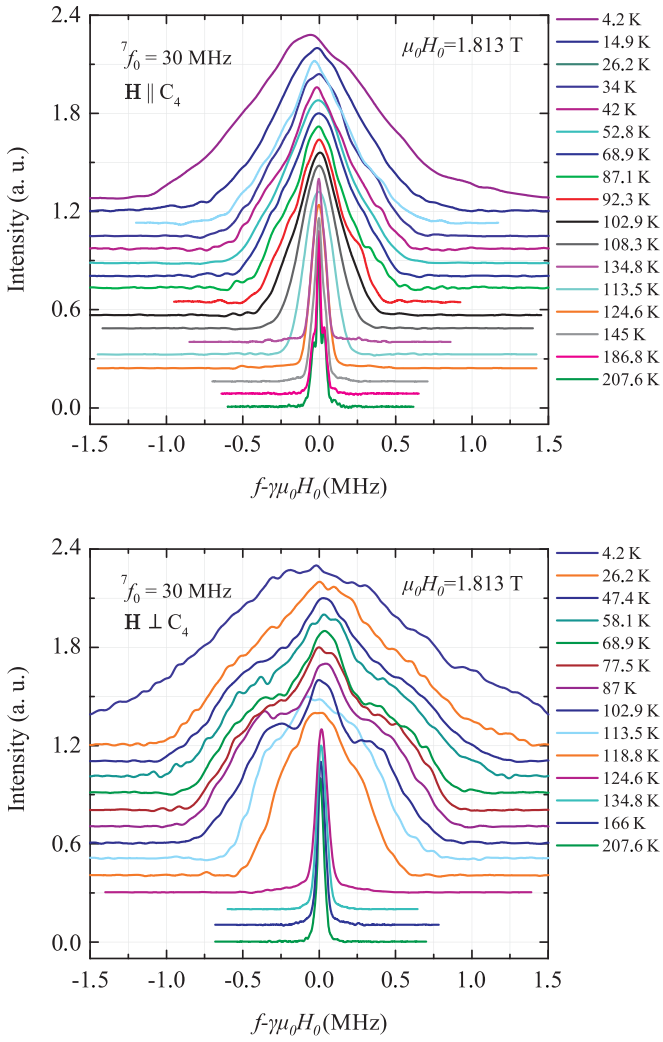

FIG. 9. Temperature evolution of ^{7}Li NMR spectra at **H** parallel and perpendicular to the crystallographic axis C_4; $\mu_0H_0 = 1.813$ T. NMR lines are stacked along ordinate axis for clarity.

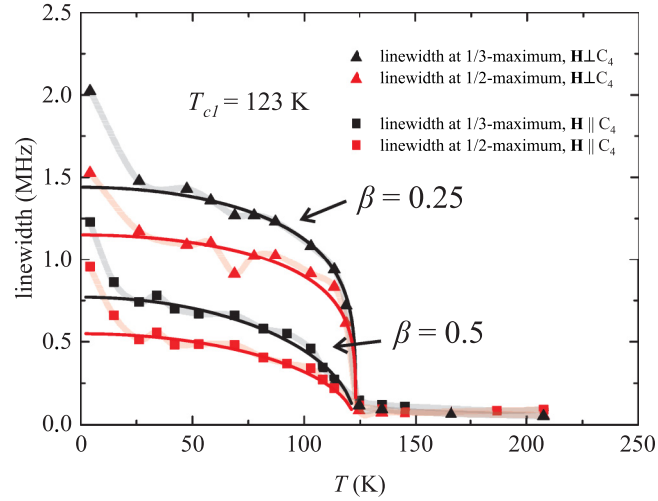

FIG. 10. Temperature dependence of ^{7}Li NMR spectra linewidth $\delta\nu(T)$ measured at 1/2 (red symbols) and 1/3 (black symbols) of maximum. Squares correspond to **H** ∥ C_4 and triangles correspond to **H** ⊥ C_4. Transparent lines are given as guides for eye. Solid lines present the fit to the power-law behavior with exponents $\beta = 0.5$ for **H** ∥ C_4 and $\beta = 0.25$ for **H** ⊥ C_4 and $T_{c1} = 123$ K.

Possible orientations of antiferromagnetic vector **l** are defined by crystal anisotropy. As far as the crystal structure of $LiCu_3O_3$ is uniaxial, in the general case, the zero-field directions of **l** will be along one of four axes lying in planes (100) and (010) or (110) and (1$\bar{1}$0) of the crystal. For both cases we can expect eight domains with equal energy at zero external field. Vectors $\mathbf{l}_{1-8}$ are shown with solid and dashed blue lines in left panel of Fig. 11.

In the special case of easy-axis anisotropy, we can expect only two domains with **l** directed along [001] and [00$\bar{1}$]. The clear observation of 90° anisotropy of magnetization measured in $LiCu_3O_3$ within the (001) plane excludes this limit case.

Angle dependencies of magnetic moment $M(\varphi)$ for low-field **H** applied in the (001) plane can be understood in the model of a strong easy-plane anisotropy and weak in-plane anisotropy.

The anisotropic part of energy of the magnetic system can be written as $D\cos^2 2\varphi - \frac{1}{2}\chi_\perp H^2 \sin^2(\varphi - \psi)$, where the first term is the in-plane anisotropy and the second term is the Zeeman energy. Here D is an in-plane anisotropy constant and $\chi_\perp$ is the magnetic susceptibility at **H** applied perpendicular to **l**. φ and ψ are the angles defining the directions of vectors **l** and **H**, respectively, counted from equilibrium direction of **l** at $H = 0$ (see right panel of Fig. 11). When the field is directed exactly between easy axes, domains $\pm l_1$ and $\pm l_2$ have equal energy. At small clockwise rotation of magnetic field, domains with $\pm\mathbf{l}_1$ will be preferable, whereas upon rotation in the other direction, domains with $\pm\mathbf{l}_2$ have lower energy. At this field direction, a spin-flop reorientation can be expected. The simple considerations of angle dependence of magnetic moment measured at different fields show that the smallest value of magnetization is expected at reorientation angle, whereas the largest one—at **H** directed along easy axis. The amplitude of magnetization modulation at field rotation in the low-field limit is expected to be close to 50% of moment measured at **H** parallel to easy axis.

The magnetization study of $LiCu_3O_3$ revealed an anomaly at **H** ∥ [110] corresponding to spin-flop reorientation. Experimental observation of spin-flop reorientation naturally

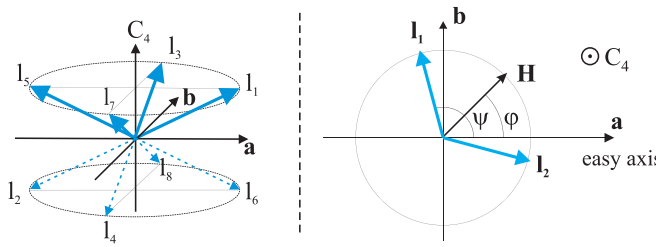

FIG. 11. (Left panel) Possible orientations of antiferromagnetic vector of model collinear structure at $H = 0$. (Right panel) Schema of a model two-domain structure with dominant easy-plane and weak in-plane anisotropies at field applied in easy plane. Angles are counted from the equilibrium direction of **l** at $H = 0$. Here, **a**, **b** mark the easy axes in plane (001).

allows us to suggest that the magnetic structure of $LiCu_3O_3$ has a uniaxial anisotropy, and axes [100] and [010] of the crystal are easy directions for the specific axis of the magnetic structure. In the contrast to collinear model antiferromagnet discussed before, the maximal modulation observed in the experiment was approximately 3% of the maximal value. Such a small value of modulation can be explained by considering the magnetic structure of $LiCu_3O_3$ as uniaxial with anisotropy of susceptibility $\chi_\parallel/\chi_\perp \approx 0.94^{\pm 1}$. Here, indexes $\parallel$ and $\perp$ correspond to mutual orientation of field and the specific axis of the uniaxial magnetic structure. Note that, in case of a usual collinear antiferromagnet, $\chi_\parallel/\chi_\perp \approx 0$ at low temperatures.

Next, we suggest more realistic model of magnetic structure of $LiCu_3O_3$ which can qualitatively explain some experimental observations, particularly the weak anisotropy of the magnetic susceptibility. The magnetic ions in $LiCu_3O_3$ have different environment of magnetic Cu^{2+} and nonmagnetic Li^+. We can evaluate the number of magnetic ions which have all four bonds in square planes between nearest magnetic ions which are marked with red crosses in our random sample of A and B planes in Fig. 2. In the A plane, we expect 32% of all sites to be occupied by such ions, whereas for the B plane the ratio is even smaller (7.8%). The number of such ions in both planes is much smaller than the percolation threshold for the square lattice [16]. Thus, ions with full set of bonds with neighbors in planes A and B form clusters joined together with magnetic ions with an incomplete set of bonds.

For A planes, clusters of ions with all four bonds are big and they all are connected via "bridges" forming an infinite cluster because the concentration of magnetic ions in A planes is higher than the percolation threshold. For B planes, clusters of ions with full set of bonds are small, and overall concentration of magnetic ions is close to the percolation threshold, which allows us to suggest that magnetic ions in B planes form weakly coupled clusters of finite sizes. Particularly, a cluster that consists of a single magnetic ion [Fig. 2(b), blue cross], as discussed before, stipulates for a sufficient part of magnetic susceptibility at low magnetic fields at $T < 30$ K.

The magnetic transition at $T_{c1} \approx 123$ K can be associated with ordering in the A planes. In the clusters with full set of bonds, one can expect the establishing of a collinear structure with antiferromagnetic vector $\mathbf{l}$ directed along one of the easy axes (as discussed before). "Bridges" of magnetic structure that have not all four bonds possibly form a noncollinear structure either due to the frustration of magnetic bonds, or because they connect collinearly ordered areas with different orientations of $\mathbf{l}$. Thus, magnetic state in the A planes can be considered as a multidomain structure with strongly developed domain walls: the number of magnetic ions forming the domain walls can be roughly evaluated as the number of ions with an incomplete number of bonds, i.e., ≈60% of magnetic ions in the A plane. Application of a sufficiently strong magnetic field must decrease the number of possible directions of $\mathbf{l}$ in magnetic domains, although complete monodomainization of the magnetic structure is impossible because magnetic field interacts with domains with $\mathbf{l}$ and $-\mathbf{l}$ equally.

The low-temperature transition at $T_{c2} \approx 30$ K supposedly corresponds to magnetic ordering in the B planes. Note that the expected value of magnetic ions in these planes with full set of bonds with magnetic neighbors is equal to $0.6^5 \times 100\% = 7.8\%$. The proximity of magnetic ion concentration in the B planes to the percolation threshold allows us to suggest that connections between clusters are weak. Magnetic order in clusters of different sizes can occur at different temperatures, so the magnetic ordering takes place over a broad temperature range, which is the reason it does not manifest itself as an abrupt singularity on temperature dependencies of magnetization and NMR linewidth. It is also possible that the ordering in the B planes has imposed a character due to the interaction with ordered neighboring A planes.

^{7}Li NMR spectra demonstrate drastic line broadening at $T < T_{c1}$, which can be ascribed to the occurrence of static magnetic moments on Cu^{2+} ions. These moments create an effective field $\Delta\mathbf{h}$ at ^{7}Li nuclei which leads to the shift of NMR frequency on $\gamma\Delta h_H$. Here, Δh_H is a projection of the local field $\Delta\mathbf{h}$ in the direction of the external magnetic field $\mathbf{H_0}$.

For modeling the NMR spectra, only dipole fields from Cu^{2+} magnetic ions from the first coordination spheres of Li^+ ions were considered. Such a suggestion was previously justified for related noncollinear structures in $LiCuVO_4$ and $RbFeMoO_4$ [25,26]. We also assumed that the values of all Cu^{2+} magnetic moments were the same.

Two different model structures were considered: the model with the ordered moments directions randomly distributed within the square plane perpendicular to the C_4 axis and the model with ordered moments directions randomly distributed in space. ^{7}Li NMR spectra calculated in frames of listed suggestions are presented in the upper panel of Fig. 12 with a red line. They are in agreement with the spectrum obtained experimentally at the lowest temperature $T = 4.2$ K shown in the same figure with a black line. The shapes of the calculated spectra were the same for both models with values of Cu^{2+} magnetic moments equal to 0.4 μ_B for the planar structure and 0.6 μ_B for the model of moments randomly directed in space. The width of individual NMR lines used for computations was $\delta\nu = 0.045$ MHz. In the inset to Fig. 12, the schema of nearest to Li^+ randomly directed moments of Cu^{2+} is presented. Li^+ is marked with open circle. Square lattice sites are marked with blue for ions from the A plane and red for ions from the B plane. In the frames of these models, neighboring positions of Li-ions were randomly occupied with magnetic Cu^{2+} and nonmagnetic Li^+ ions, in accordance with the occupation probability in the A and B planes. Strong spin reduction in low-dimensional $S = 1/2$ systems is natural: for related magnets Sr_2CuO_3 and $LiCuVO_4$, magnetic moment value is 0.06 μ_B and 0.31 μ_B, respectively [27,28].

At higher temperatures, NMR lines have a more complicated shape. An experimental spectrum obtained at $T = 47.4$ K is shown by the black line in the bottom panel of Fig. 12 and a model spectrum is shown by the red line. The value of the magnetic moment used in calculations was 0.4 μ_B. The schema of suggested magnetic structure is given in the inset to Fig. 12. At this temperature, we suppose that spins from the B plane are not ordered. In the A plane, the directions of the closest magnetic moments are suggested to be correlated antiparallel and lying within the plane perpendicular to C_4, but their directions within the plane are arranged randomly. This model partially describes the experimental spectrum at this temperature. The nonshifted

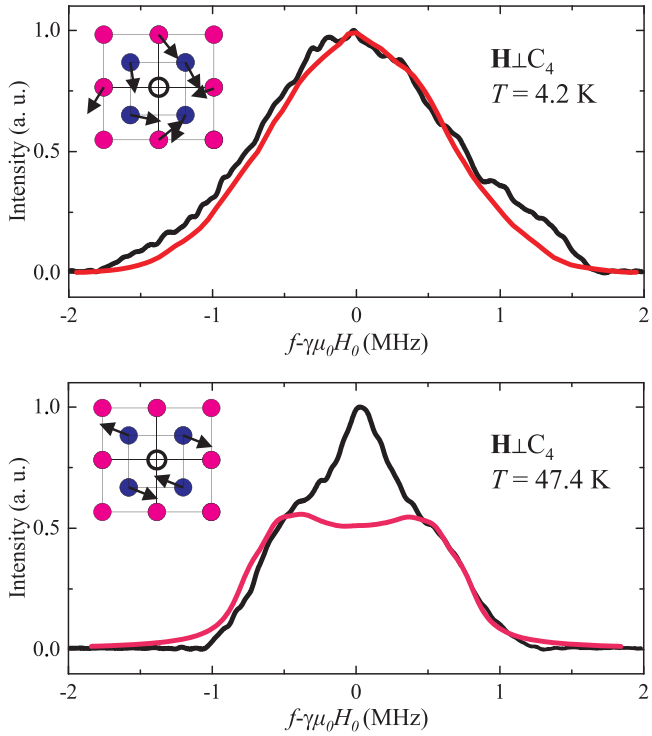

FIG. 12. The results of modeling ^{7}Li NMR spectra, $\mathbf{H} \perp C_4$ from Fig. 9. Black lines show experimental spectra obtained at $T = 4.2$ K (top panel) and $T = 47.4$ K (bottom panel). Corresponding red lines show spectra calculated in frames of the models described in text. Insets show the model orientation of magnetic moments in crystallographic planes A (blue circles) and B (magenta circles).

peak can probably be explained by the signal from Li^+ surrounded by strongly reduced magnetic moments. The integral intensity of this peak is about 15% of the total NMR line intensity.

Here, we did not consider the possibility of the frustration of exchange interactions, which can play a significant role in the formation of a frozen disordered structure. Hence, on the example of the frustrated SLQAF system Li_2VOSiO_4 it was shown that doping with nonmagnetic Ti^{4+} impurities sufficiently influences the frustration of exchange interactions [11]. In geometrically frustrated quasi-2D magnets with a triangular lattice one can expect the establishment of a disordered spin-glass-like state even at 10%–20% depletion of the magnetic system with nonmagnetic ions [29]. Studies of magnetic properties of $CuCrO_2$, an example of quasi-2D antiferromagnets with triangular lattice, doped with vanadium—$CuCr_{1-x}V_xO_2$—revealed a spin-glass state at the doping level of 8% [30,31]. Studies of another quasi-2D magnet, $Rb_{1-x}K_xFe(MoO4)_2$, showed that samples with a doping of 15% ($x = 0.15$) present frozen magnetic disorder [32].

VI. CONCLUSION

In this work, a novel quasi-2D antiferromagnet with a randomly depleted square lattice of spins $S = 1/2$ was studied. ^{7}Li NMR and magnetization measurements performed on single crystals of $LiCu_3O_3$ revealed the occurrence of magnetic order at $T_{c1} = 123$ K and the change of the magnetic state at $T_{c2} \approx 30$ K. We ascribe the high-temperature transition to the establishment of magnetic order in planes with a higher concentration of magnetic ions and a low-temperature transition to the magnetic ordering in planes with lower concentration of magnetic ions. Broad continuous NMR spectra below T_{c1} reflect a continuous distribution of magnetic moments in $LiCu_3O_3$, which is typical for spiral, spin-modulated magnetic structures or structures with frozen disorder. Magnetization measurements revealed a spin-flop transition which indicates weak uniaxial anisotropy of spin structure with susceptibilities $\chi_\parallel/\chi_\perp \approx 0.94$. Fourth-order anisotropy with easy axes directed along the [100] and [010] axes of the crystal was observed. The small magnetic susceptibility for all orientations of applied magnetic field shows that magnetic structure is rigid since the estimated value of the saturation field derived from the differential susceptibility measured at $\mu_0 H = 5$ T is $\mu_0 H_{\text{sat}} \approx 200$ T.

ACKNOWLEDGMENTS

We thank V. I. Marchenko, S. S. Sosin, and M. Zhitomirsky for stimulating discussions and L. B. Lugansky for data processing assistance. The work was financially supported by the Russian Science Foundation Grant No. 22-12-00259 (NMR data processing and calculations); and the Basic Research Program of HSE (magnetization data processing). Part of the work (on single crystals growth) performed at the MIREA RTU was funded by the Ministry of Science and Higher Education of the Russian Federation within the framework of the State Task (FSFZ-2023-0005 project).

[1] R. Melzi, P. Carretta, A. Lascialfari, M. Mambrini, M. Troyer, P. Millet, and F. Mila, $Li_2VO(Si, Ge)O_4$, a Prototype of a two-dimensional frustrated quantum Heisenberg antiferromagnet, Phys. Rev. Lett. **85**, 1318 (2000).

[2] R. Melzi, S. Aldrovandi, F. Tedoldi, P. Carretta, P. Millet, and F. Mila, Magnetic and thermodynamic properties of Li_2VOSiO_4: A two-dimensional $S = 1/2$ frustrated antiferromagnet on a square lattice, Phys. Rev. B **64**, 024409 (2001).

[3] G. Shirane, Y. Endoh, R. J. Birgeneau, M. A. Kastner, Y. Hidaka, M. Oda, M. Suzuki, and T. Murakami, Two-dimensional antiferromagnetic quantum spin-fluid state in La_2CuO_4, Phys. Rev. Lett. **59**, 1613 (1987).

[4] Y. Endoh, K. Yamada, R. J. Birgeneau, D. R. Gabbe, H. P. Jenssen, M. A. Kastner, C. J. Peters, P. J. Picone, T. R. Thurston, J. M. Tranquada, G. Shirane, Y. Hidaka, M. Oda, Y. Enomoto, M. Suzuki, and T. Murakami, Static and dynamic spin correlations in pure and doped La_2CuO_4, Phys. Rev. B **37**, 7443 (1988).

[5] O. P. Vajk, P. K. Mang, M. Greven, P. M. Gehring, and J. W. Lynn, Quantum impurities in the two-dimensional spin one-half Heisenberg antiferromagnet, Science **295**, 1691 (2002).

[6] K. Kato, S. Todo, K. Harada, N. Kawashima, S. Miyashita, and H. Takayama, Quantum phase transition of the randomly diluted Heisenberg antiferromagnet on a square lattice, Phys. Rev. Lett. **84**, 4204 (2000).

[7] A. W. Sandvik, Classical percolation transition in the diluted two-dimensional $S = 1/2$ Heisenberg antiferromagnet, Phys. Rev. B **66**, 024418 (2002).

[8] A. L. Chernyshev, Y. C. Chen, and A. H. Castro Neto, Diluted quantum antiferromagnets: Spin excitations and long-range order, Phys. Rev. B **65**, 104407 (2002).

[9] S. Liu and A. L. Chernyshev, Impurity-induced frustration: Low-energy model of diluted oxides, Phys. Rev. B **87**, 064415 (2013).

[10] P. Carretta, G. Prando, S. Sanna, R. De Renzi, C. Decorse, and P. Berthet, Evidence for impurity-induced frustration in La_2CuO_4, Phys. Rev. B **83**, 180411(R) (2011).

[11] N. Papinutto and P. Carretta, S. Gonthier, and P. Millet, Spin dilution in frustrated two-dimensional $S = 1/2$ antiferromagnets on a square lattice, Phys. Rev. B **71**, 174425 (2005).

[12] S. J. Hibble, J. Kohler, A. Simon, and S. Paider, $LiCu_2O_2$ and $LiCu_3O_3$: New mixed valent copper oxides, J. Solid State Chem. **88**, 534 (1990).

[13] A. A. Bush, K. E. Kamentsev, and E. A. Tishchenko, Growth and properties of $LiCu_2O_2$-$NaCu_2O_2$ crystals, Inorg. Mater. **55**, 374 (2019).

[14] R. Berger, P. Önnerud, and R. Tellgren, Structure refinements of $LiCu_2O_2$ and $LiCu_3O_3$ from neutron powder diffraction data, J. Alloys Compd. **184**, 315 (1992).

[15] T. Masuda, A. Zheludev, B. Roessli, A. Bush, M. Markina, and A. Vasiliev, Spin waves and magnetic interactions in $LiCu_2O_2$, Phys. Rev. B **72**, 014405 (2005).

[16] J. M. Ziman, *Models of Disorder: The Theoretical Physics of Homogeneously Disordered Systems* (Cambridge University Press, Cambridge, 1979).

[17] D. A. Balaev, A. A. Krasikov, A. A. Dubrovskii, S. V. Semenov, O. A. Bayukov, S. V. Stolyar, R. S. Iskhakov, V. P. Ladygina, and L. A. Ishchenko, Magnetic properties and the mechanism of formation of the uncompensated magnetic moment of antiferromagnetic ferrihydrite nanoparticles of a bacterial origin, J. Exp. Theor. Phys. **119**, 479 (2014).

[18] A. M. Vorotynov, A. I. Pankrats, G. A. Petrakovskii, K. A. Sablina, W. Paszkowicz, and H. Szymczak, Magnetic and resonance properties of $LiCu_2O_2$ single crystals, J. Exp. Theor. Phys. **86**, 1020 (1998).

[19] N. Büttgen, H.-A. Krug von Nidda, L. E. Svistov, L. A. Prozorova, A. Prokofiev, and W. Aßmus, Spin-modulated quasi-one-dimensional antiferromagnet $LiCuVO_4$, Phys. Rev. B **76**, 014440 (2007).

[20] V. N. Glazkov, Yu. V. Krasnikova, I. K. Rodygina, H.-A. Krug von Nidda, T. Masuda, M. Hemmida, and M. Hirrle, Magnetic resonance in the quasi-2D square lattice easy-plane antiferromagnet $Ba_2MnGe_2O_7$, J. Exp. Theor. Phys. **137**, 542 (2023).

[21] Yu. A. Sakhratov, J. J. Kweon, E. S. Choi, H. D. Zhou, L. E. Svistov, and A. P. Reyes, Search for a nematic phase in the quasi-two-dimensional antiferromagnet $CuCrO_2$ by NMR in an electric field, Phys. Rev. B **97**, 094409 (2018).

[22] Yu. A. Sakhratov, L. E. Svistov, P. L. Kuhns, H. D. Zhou, and A. P. Reyes, Magnetic structure and domain conversion of the quasi-2D frustrated antiferromagnet $CuCrO_2$ probed by NMR, J. Exp. Theor. Phys. **119**, 880 (2014).

[23] P. Chandra, P. Coleman, and A. I. Larkin, Ising transition in frustrated Heisenberg models, Phys. Rev. Lett. **64**, 88 (1990).

[24] V. E. Valiulin, A. V. Mikheyenkov, N. M. Chtchelkatchev, and A. F. Barabanov, Continuous transformation between ferro and antiferro circular structures in $\boldsymbol{J_1 - J_2 - J_3}$ frustrated Heisenberg model, J. Phys.: Condens. Matter **31**, 455801 (2019).

[25] N. Büttgen, W. Kraetschmer, L. E. Svistov, L. A. Prozorova, and A. Prokofiev, NMR study of the high-field magnetic phase of $LiCuVO_4$, Phys. Rev. B **81**, 052403 (2010).

[26] T. A. Soldatov, Yu. A. Sakhratov, L. E. Svistov, and A. I. Smirnov, Triangular antiferromagnet $RbFe(MoO_4)_2$ with the replacement of nonmagnetic ions, J. Exp. Theor. Phys. **131**, 62 (2020).

[27] K. M. Kojima, Y. Fudamoto, M. Larkin, G. M. Luke, J. Merrin, B. Nachumi, Y. J. Uemura, N. Motoyama, H. Eisaki, S. Uchida, K. Yamada, Y. Endoh, S. Hosoya, B. J. Sternlieb, and G. Shirane, Reduction of ordered moment and Néel temperature of quasi-one-dimensional antiferromagnets Sr_2CuO_3 and Ca_2CuO_3, Phys. Rev. Lett. **78**, 1787 (1997).

[28] B. J. Gibson, R. K. Kremer, A. V. Prokofiev, W. Assmus, and G. J. McIntyre, Incommensurate antiferromagnetic order in the $S = 1/2$ quantum chain compound $LiCuVO_4$, Phys. B (Amsterdam, Neth.) **350**, E253 (2004).

[29] Z. R. Yan, M. H. Qin, S. Dong, M. Zeng, X. B. Lu, X. S. Gao, and J.-M. Liu, Spin glass state and enhanced spiral phase in doped delafossite oxide $CuCrO_2$, Phys. Rev. B **94**, 024410 (2016).

[30] K. Singh, A. Maignan, Ch. Simon, S. Kumar, C. Martin, O. Lebedev, S. Turner, and G. Van Tendeloo, Magnetodielectric $CuCr_{0.5}V_{0.5}O_2$: An example of a magnetic and dielectric multiglass, J. Phys.: Condens. Matter **24**, 226002 (2012).

[31] S. Kumar, K. Singh, M. Miclau, Ch. Simon, C. Martin, and A. Maignan, From spin induced ferroelectricity to spin and dipolar glass in a triangular lattice: The $CuCr_{1-x}V_xO_2$ ($0 \leqslant x \leqslant 0.5$) delafossite, J. Solid State Chem. **203**, 37 (2013).

[32] Yu. A. Sakhratov, M. Prinz-Zwick, D. Wilson, N. Büttgen, A. Ya. Shapiro, L. E. Svistov, and A. P. Reyes, Magnetic structure of the triangular antiferromagnet $RbFe(MoO_4)_2$ weakly doped with nonmagnetic K^+ ions studied by NMR, Phys. Rev. B **99**, 024419 (2019).